Quaternary Research (2018), **89**, 619–628.

doi:10.1017/qua.2017.77

SPECIAL ISSUE
INQUA LoessFest 2016

Mineral magnetic record of the Miocene-Pliocene climate transition on the Chinese Loess Plateau, North China

Hong Ao[a,b]*, Mark J. Dekkers[c], Andrew P. Roberts[d], Eelco J. Rohling[d,e], Zhisheng An[a], Xiaodong Liu[a], Zhaoxia Jiang[f], Xiaoke Qiang[a], Yong Xu[g], Hong Chang[a]

[a]State Key Laboratory of Loess and Quaternary Geology, Institute of Earth Environment, Chinese Academy of Sciences, Xi'an 710061, China
[b]Lamont-Doherty Earth Observatory, Columbia University, Palisades, New York 10964, USA
[c]Paleomagnetic Laboratory 'Fort Hoofddijk', Department of Earth Sciences, Faculty of Geosciences, Utrecht University, Budapestlaan 17, 3584 CD Utrecht, The Netherlands
[d]Research School of Earth Sciences, The Australian National University, Canberra 2601, Australia
[e]Ocean and Earth Science, National Oceanography Centre, University of Southampton, Southampton SO14 3ZH, United Kingdom
[f]State Key Laboratory of Lithospheric Evolution, Institute of Geology and Geophysics, Chinese Academy of Sciences, Beijing 100029, China
[g]Xi'an Center of Geological Survey, China Geological Survey, Xi'an 710054, China

(Received March 28, 2017; Accepted August 13, 2017)

Abstract

Pre-Quaternary terrestrial climate variability is less well understood than that during the Quaternary. The continuous eolian Red Clay sequence underlying the well-known Quaternary loess-paleosol sequence on the Chinese Loess Plateau (CLP) provides an opportunity to study pre-Quaternary terrestrial climate variability in East Asia. Here, we present new mineral magnetic records for a recently found Red Clay succession from Shilou area on the eastern CLP, and demonstrate a marked East Asian climate shift across the Miocene-Pliocene boundary (MPB). Pedogenic fine-grained magnetite populations, ranging from superparamagnetic (SP)/single domain (SD) up to small pseudo-single domain (PSD) sizes (i.e., from <30 nm up to ~1000 nm), dominate the magnetic properties. Importantly, our mineral magnetic results indicate that both pedogenic formation of SP grains and transformation of SP grains to SD and small PSD grains accelerated across the MPB in the Shilou Red Clay, which are indicative of enhanced pedogenesis. We relate this enhanced pedogenesis to increased soil moisture availability on the CLP, associated with stronger Asian Summer Monsoon precipitation during an overall period of global cooling. Our study thus provides new insights into the Miocene-Pliocene climate transition in East Asia.

Keywords: Environmental magnetism; Chinese Loess Plateau; Red clay; Paleoclimate; Asian Summer Monsoon; Miocene-Pliocene transition

INTRODUCTION

The Chinese Loess Plateau (CLP) hosts a vast expanse (~300,000 km^2) of thick eolian dust deposits that provide a globally outstanding terrestrial archive of Late Cenozoic climatic and environmental changes (Liu, 1985; An, 2014). These eolian deposits can be divided into two parts: the well-known Quaternary loess-paleosol sequence and the underlying Miocene-Pliocene Red Clay sequence. While the climatic history recorded by Quaternary loess-paleosol sequences is relatively well constrained, the climatic significance of Red Clay sequences is far from established (An, 2014; Ao et al., 2016; Nie et al., 2016). Existing Miocene-Pliocene paleoclimate records from the semi-arid CLP (An et al., 2001, 2005; Nie et al., 2014; Ao et al., 2016), arid western China (Miao et al., 2012), and humid South China (Clift et al., 2014) provide contrasting information on climate variability over this time interval.

Formation of fine magnetic grains (from <30 nm up to ~1000 nm) in the Chinese loess-paleosol and Red Clay deposits, including superparamagnetic (SP), stable single domain (SD), and small pseudo-single-domain (PSD) particles, is closely linked to *in situ* pedogenic weathering modulated by climate and can be quantified using magnetic techniques (Zhou et al., 1990; An et al., 1991; Verosub et al., 1993; Evans and Heller, 1994; Heller and Evans, 1995; An et al., 2001; Liu et al., 2003, 2004; Bloemendal and Liu, 2005;

*Corresponding author at: State Key Laboratory of Loess and Quaternary Geology, Institute of Earth Environment, Chinese Academy of Sciences, Xi'an 710061, China. Lamont-Doherty Earth Observatory, Columbia University, Palisades, New York 10964, USA. E-mail address: aohong@ieecas.cn.

Nie et al., 2008; Ao et al., 2016). Therefore, magnetic parameters are widely used to investigate pedogenic weathering, monsoon evolution, aridification history, and global climate change recorded in Quaternary loess-paleosol sequences (Kukla et al., 1988; An et al., 1991; Verosub et al., 1993; Florindo et al., 1999; Evans and Heller, 2001; Deng et al., 2005, 2006; Liu et al., 2007, 2012, 2013, 2015). However, considerably less environmental magnetic research has focused on the underlying Miocene-Pliocene Red Clay sequences (Nie et al., 2016). Here, we investigate late Miocene-early Pliocene climate change in East Asia; new mineral magnetic records of a Red Clay succession from Shilou (36°55' N, 110°56' E) on the eastern CLP form the basis for our paleoclimatic interpretations.

GENERAL SETTING

The Asian monsoon, which is the most dynamic component of the global monsoon system, is characterized by seasonal reversal of winter and summer monsoons (Webster, 1994; Wang et al., 2005; An et al., 2015). The Asian Winter Monsoon (AWM) transports cold and dry air from high-latitude Eurasia toward South China, while the Asian Summer Monsoon (ASM) transports heat and moisture from the equatorial oceans to North China (Wang et al., 2005; An et al., 2015).

The Shilou Red Clay section lies between the Lüliang Mountains and the Yellow River on the eastern CLP, at the northern margin of ASM influence (Fig. 1). The climate and environment of the Shilou area are dominated by a seasonal reversal of AWM and ASM circulations. This region today has a mean annual temperature of ~9°C and mean annual precipitation of ~500 mm, with over 60% of the precipitation falling in the summer. The Shilou Red Clay sequence has a thickness of up to ~90 m and ranges in age from ~8.2 to 2.6 Ma (Ao et al., 2016). In general, the horizontally stratified Shilou Red Clay consists of reddish soils that are intercalated with carbonate nodules (Fig. 1c). It has a redder color and has experienced stronger pedogenesis than the overlying Quaternary loess-paleosol sequence (Fig. 1c).

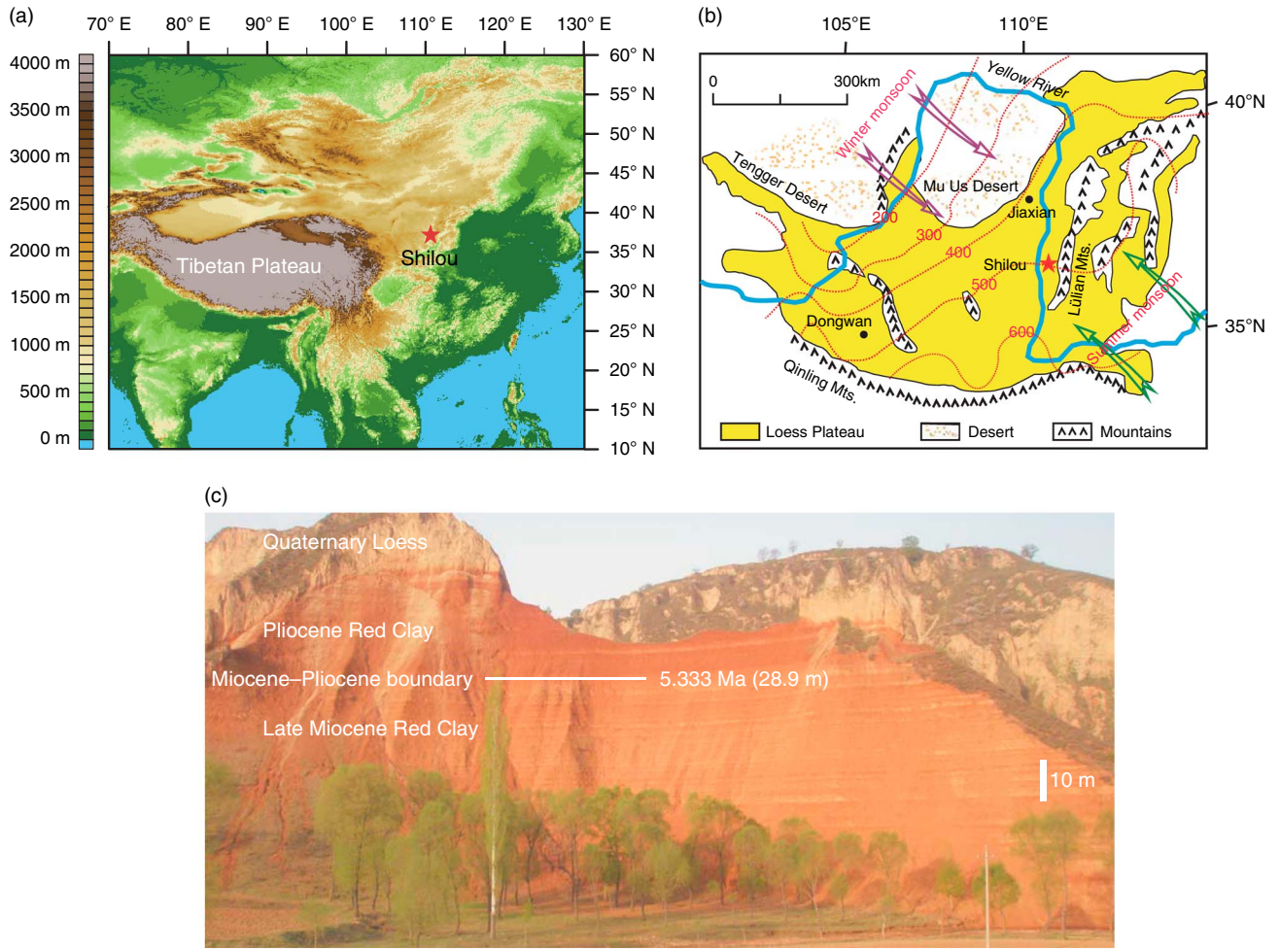

Figure 1. (color online) Schematic map of the site location and geological setting. (a) Map of Asian topography. (b) Map of the Chinese Loess Plateau with location of the studied Shilou red clay section. The Yellow River is the major river system in North China. The dashed red lines denote contours of mean annual precipitation (mm) on the Chinese Loess Plateau. (c) Field photograph of the Shilou-A red clay section. The upper part (Pliocene) has a distinctly redder color than the lower part (Late Miocene), which is consistent with enhanced pedogenesis and increased summer monsoon precipitation across the Miocene-Pliocene boundary.

https://doi.org/10.1017/qua.2017.77 Published online by Cambridge University Press

This study focuses on the ~70-m-thick Shilou Red Clay section studied by Xu et al. (2009) (here named the Shilou-A section), which is located ~1 km east of our recently investigated section with ~90-m-thick Shilou Red Clay (here referred to as the Shilou-B section; Ao et al., 2016). Two previous correlations of the Shilou-A magnetostratigraphy to the geomagnetic polarity timescale (GPTS) suggest contrasting ages of ~11–2.6 Ma (from polarity subchron C5n.2n to C2An.1n; Xu et al., 2009) and ~5.2–2.6 Ma (from C3n.4n to C2An.1n; Anwar et al., 2015) for the ~70-m-thick Shilou Red Clay sequence. However, these magnetostratigraphic interpretations both involve ambiguous polarity divisions, which result in poor and equivocal correlations to the GPTS. Furthermore, these age assignments (~11–2.6 Ma or ~5.2–2.6 Ma) are inconsistent with the generally accepted age from ~8–7 Ma to 2.6 Ma for the Red Clay sequences on the central and eastern CLP (Sun et al., 1998; Ding et al., 1999; Qiang et al., 2001). In addition, the age assignment of ~5.2–2.6 Ma (Anwar et al., 2015) is not supported by the presence of the late Miocene micromammal *Meriones* sp. in the lower Shilou-A section at 46.6 m (Xu et al., 2012). Our recent magnetostratigraphy from the 90-m-thick Shilou-B section (Ao et al., 2016), with a much higher resolution and significantly improved definition of respective polarity zones, enables unequivocal magnetostratigraphic correlation (C4r.1r–C2An.1n, ~8.2–2.6 Ma) to the GPTS. This results in a revised correlation of the ~70-m-thick Shilou-A magnetostratigraphy to the GPTS from C4n.2n to C2An.1n (~8–2.6 Ma). Thus, a chronology from 3.6 to 7.5 Ma (12.2–60.4 m) for the late Miocene-early Pliocene Shilou Red Clay within the ~70-m-thick Shilou-A succession is established based on our updated magnetostratigraphic correlation (Ao et al., 2016). The chronology was constructed via linear interpolation using geomagnetic polarity reversals for age control, assuming constant long-term sedimentation rates between reversals (Fig. 2).

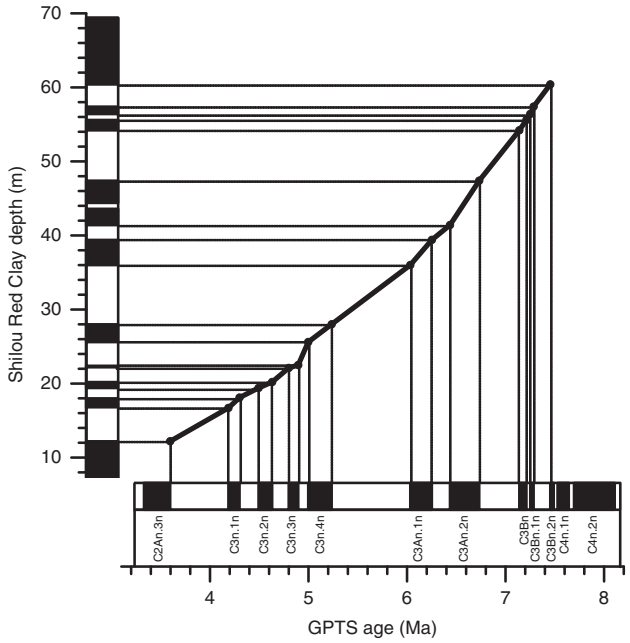

Figure 2. Age-depth model for the 12.2–60.4 m interval of the Shilou-A red clay succession established from the updated magnetostratigraphic correlation (Ao et al., 2016) to the geomagnetic polarity timescale (GPTS; Hilgen et al., 2012).

SAMPLING AND METHODS

After removal of the weathered outcrop surface, 703 fresh samples were collected from the whole (~70-m-thick) Shilou-A Red Clay succession at 10 cm stratigraphic intervals (equivalent to a time spacing of ~8 ka). A total of 473 samples from the 12.2–60.4 m interval (3.6 to 7.5 Ma) were selected for the present study. Samples were powdered and then packed into non-magnetic cubic boxes for low-frequency magnetic susceptibility (χ_{lf}) measurements in the laboratory. χ_{lf} was measured with a Bartington Instruments MS2 magnetic susceptibility meter at 470 Hz. An anhysteretic remanent magnetization (ARM) was imparted using a peak alternating field (AF) of 100 mT and a 0.05 mT direct current (DC) bias field, and was measured using a 2-G Enterprises superconducting rock magnetometer (model 755R) housed in a magnetically shielded room. ARM is expressed in terms of the ARM susceptibility (χ_{ARM}), which was obtained by dividing ARM intensity by the DC field strength.

Temperature-dependent susceptibility (χ-T) curves were measured in an argon atmosphere (with an argon flow rate of 100 mL/min) from room temperature to 700°C and back to room temperature using a MFK1-FA susceptometer equipped with a CS-3 high-temperature furnace (AGICO, Brno, Czech Republic). A χ run with an empty furnace tube was measured to determine the temperature-dependent background before measuring the sediment samples. The susceptibility of each sediment sample was obtained by subtracting the measured furnace tube background χ using the CUREVAL 5.0 program (AGICO, Brno, Czech Republic). Isothermal remnant magnetization (IRM) acquisition curves were measured at 30 field steps up to a maximum field of 2 T. Samples were magnetized with an ASC IM-10-30 pulse magnetizer, and IRMs were measured with an AGICO JR-6A spinner magnetometer. First-order reversal curve (FORC) measurements (Roberts et al., 2000, 2014) were made using the variable resolution FORC protocol (Zhao et al., 2015) with a Princeton Measurements Corporation (Model 3900) vibrating sample magnetometer (VSM). For each sample, 80 FORCs were measured at fields up to 300 mT with an averaging time of 200 ms. Data were processed using the software of Zhao et al. (2015) with a smoothing factor of 3.

RESULTS

Heating and cooling χ-T curves are nearly reversible (Fig. 3), which indicates that little magnetic mineral transformation occurred during thermal treatment (Ao et al., 2009). All of the

https://doi.org/10.1017/qua.2017.77 Published online by Cambridge University Press

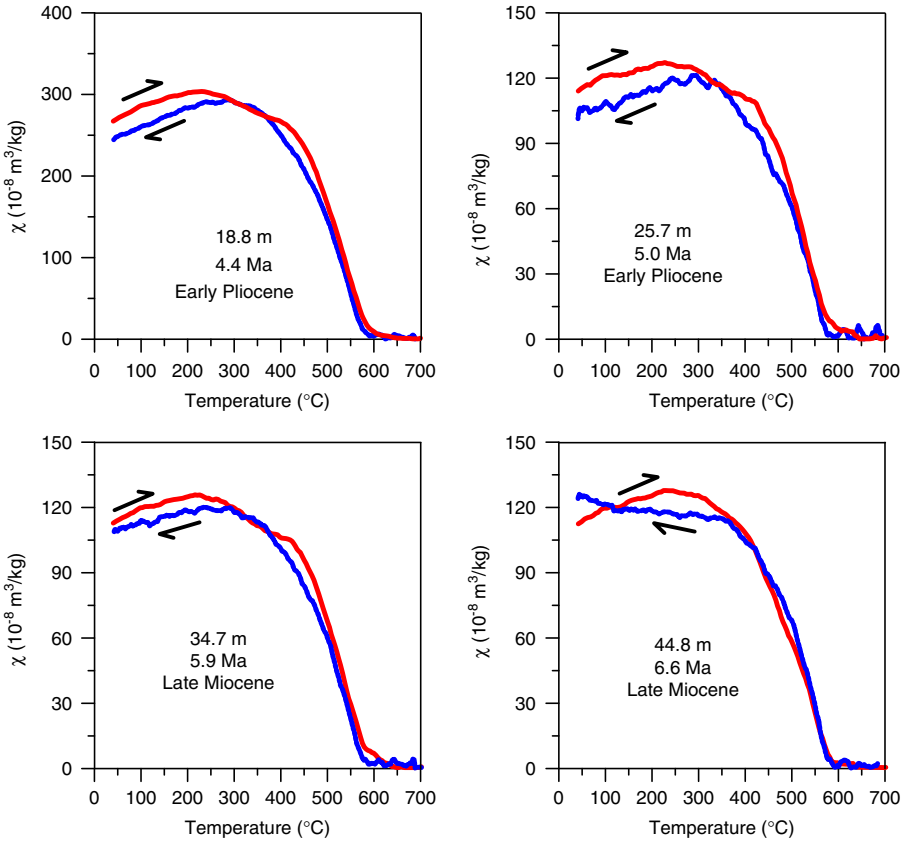

Figure 3. (color online) χ-T curves for selected samples from the Shilou-A red clay sequence. The red and blue lines represent heating and cooling curves, respectively.

heating curves are characterized by a major inflection at ~580°C, which corresponds to the Curie temperature of magnetite and is consistent with the ubiquitous presence of magnetite in Red Clay (Liu et al., 2003; Xu et al., 2009; Ao et al., 2016). A steady increase in χ from room temperature to ~200–300°C indicates the gradual unblocking of fine (SP/SD) magnetite particles (Liu et al., 2005, 2010; Deng, 2008). There was no magnetic mineral transformation during heating, so the slight drop in χ to ~400°C is possibly due to changes in crystallinity, grain size, or morphology of magnetic particles (Dunlop and Özdemir, 1997; Ao et al., 2012).

The measured IRM acquisition curves are characterized by a major increase below 300 mT (Fig. 4), which supports the interpretation of a dominant contribution from magnetite. The slight increase between 300 and 2000 mT is consistent with the presence of hematite. On a mass-specific basis, hematite has a much weaker magnetization than magnetite (Dunlop and Özdemir, 1997), thus large hematite concentrations are necessary to contribute substantially to IRM when magnetite is also present.

All FORC diagrams have closed contours with maximum contour density at a B_c value of ~10 mT (Fig. 5), which indicates a substantial presence of SD magnetite (Roberts et al., 2000, 2014; Egli et al., 2010). The outer contours are generally divergent along the B_u axis, which points to a small PSD component (Roberts et al., 2000, 2014; Muxworthy and Dunlop, 2002).

Magnetic parameters (e.g., χ_{ARM} and χ_{lf}) and their ratios are sensitive indicators of changes in magnetic mineralogy and are useful for establishing high-resolution paleoclimatic records because such parameters can be good proxies for important paleoenvironmental and paleoclimatic processes (Evans and Heller, 2003; Liu et al., 2012, 2015). For the Shilou-A Red Clay sequence, χ_{ARM} and χ_{lf} have consistent variations, which are characterized by a prominent shift to higher values across the Miocene-Pliocene boundary (MPB, 5.333 Ma; Fig. 6a and b). Such a shift across the MPB is better characterized in the adjacent χ_{ARM}/χ_{lf} record (Fig. 6c): χ_{ARM}/χ_{lf} increases significantly from ~4.1 at ~5.6 Ma to ~7.0 at ~5 Ma. Overall, χ_{ARM}/χ_{lf} ranges from 3.3 to 6.2 (average 5.2) during the late Miocene (7.5–5.333 Ma) and from 4.7 to 7.0 (average 5.8) during the early Pliocene (5.333–3.6 Ma; Fig. 6c). Such a χ_{ARM}/χ_{lf} shift is also observed in our recently investigated Shilou-B section across the MPB (Ao et al., 2016; Fig. 6d). The two χ_{ARM}/χ_{lf} records have generally consistent variability, particularly over longer periods. Minor differences between them are probably related to different sampling intervals (10 cm sampling interval in the ~70-m-thick Shilou-A succession, versus a 2-cm sampling interval in the ~90-m-thick Shilou-B succession) and minor differences in sedimentary continuity and/or short-term magnetostratigraphic age model issues.

https://doi.org/10.1017/qua.2017.77 Published online by Cambridge University Press

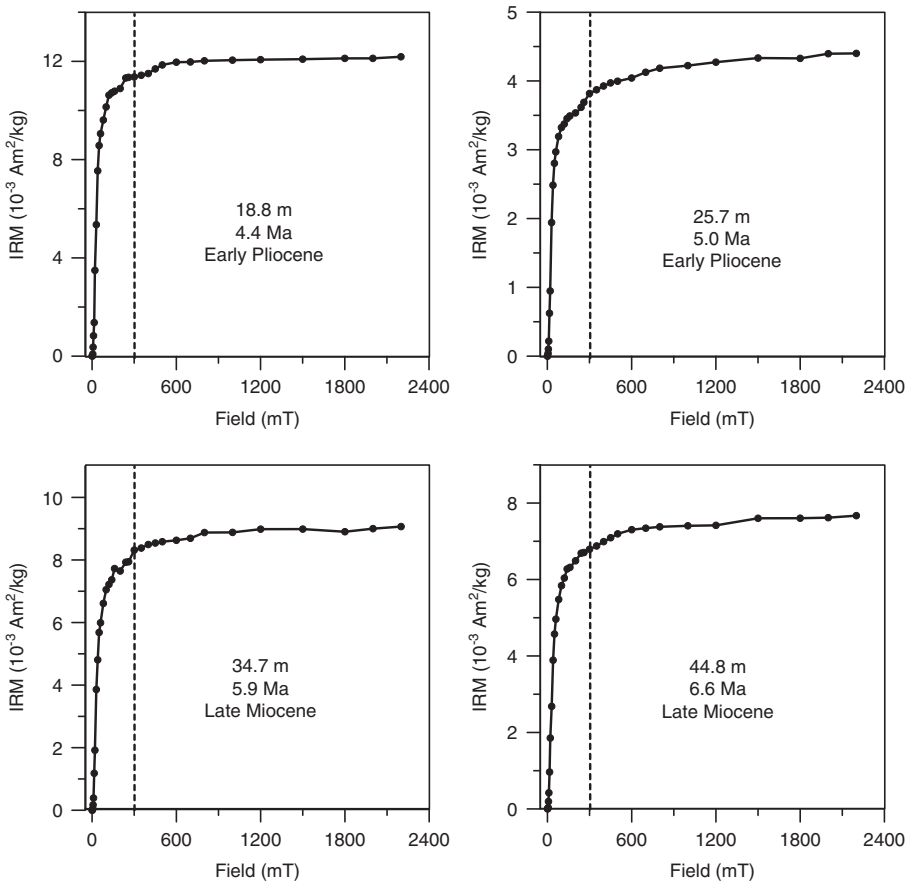

Figure 4. IRM acquisition curves for selected samples from the Shilou-A red clay sequence (the same samples as in Fig. 3). The dashed vertical lines at 300 mT are shown to aid distinction between low-and high-coercivity portions of the IRM acquisition curves.

DISCUSSION

Like the overlying Quaternary loess-paleosol sequence, the magnetic properties of the Red Clay sequence are dominated by fine-grained pedogenic magnetite populations that range from SP/SD to small PSD sizes, as suggested by the aforementioned rock magnetic results and previous studies (Nie et al., 2007, 2008, 2013; Ao et al., 2016). The SP grains, which have high χ_{lf} values but no stable magnetic remanence, formed during early pedogenesis. Some SP grains could have grown to SD and even to small PSD sizes, which have high χ_{ARM} but low χ_{lf} with increased pedogenesis (Evans and Heller, 2003; Hu et al., 2013; Nie et al., 2013, 2014). Thus, χ_{ARM}/χ_{lf}, which reflects the relative amount of SD and small PSD magnetite grains compared to SP grains, allows a more detailed view of pedogenic variations in Red Clay than either χ_{lf} or χ_{ARM} (Geiss and Zanner, 2006; Nie et al., 2013, 2014). This approach is supported by χ_{ARM}/χ_{lf} variations of Quaternary loess-paleosol sequences, with distinctly high values in pedogenic paleosol layers and low values in loess layers (Nie et al., 2013). Hematite has much lower magnetization and magnetic susceptibility than magnetite; therefore, the contribution of hematite to χ_{ARM}/χ_{lf} variations is not significant when magnetite is also present.

The notable χ_{lf} and χ_{ARM} increases across the MPB in the Shilou Red Clay indicate increases in pedogenic SP and SD to small PSD magnetite grains, respectively. An increased amount of SP magnetite grains is supported by a notable increase in the frequency-dependent magnetic susceptibility percentage (χ_{fd}%, defined as $(\chi_{lf} - \chi_{hf}) / \chi_{lf} \times 100\%$, where χ_{hf} is the high-frequency magnetic susceptibility) in the Shilou-B Red Clay section across the MPB (Ao et al, 2016; Fig. 6e). The prominent χ_{ARM}/χ_{lf} increase across the MPB further indicates an increasing percentage of SD and small PSD magnetite grains relative to SP grains. Thus, consistent positive shifts of χ_{lf}, χ_{ARM}, χ_{ARM}/χ_{lf}, and χ_{fd}% indicate enhanced pedogenesis across the MPB on the CLP, which accelerated both formation of SP grains and transformation of SP grains to SD and small PSD grains. Relatively more SD and small PSD grains formed during this type of pedogenic enhancement, which resulted in increased χ_{ARM}/χ_{lf} across the MPB. It is unlikely that the increased PSD magnetite fraction resulted from increased detrital input, because parallel grain size records from the Shilou-A Red Clay do not indicate coarser sediments and increased detrital input across the MPB (Xu et al., 2012). In addition, the early Pliocene Shilou Red Clay interval is redder than the underlying late Miocene interval (Fig. 1c), and has more Fe-Mn (hydr)oxide mottles, nodules, concretions, and coatings in soil profiles, which are

https://doi.org/10.1017/qua.2017.77 Published online by Cambridge University Press

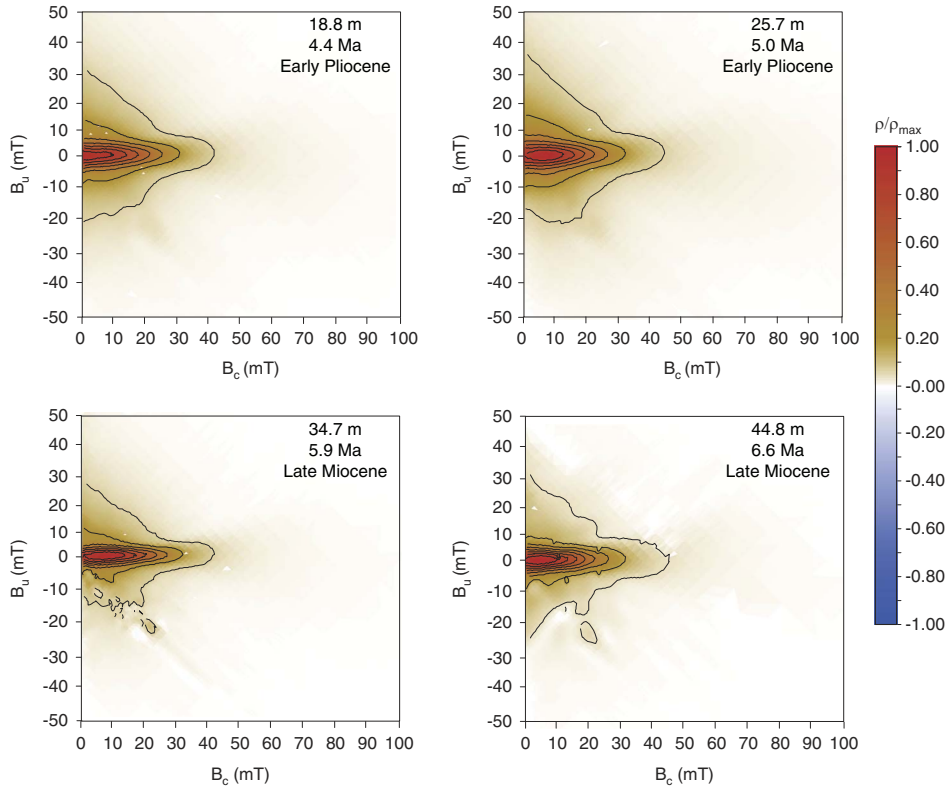

Figure 5. (color online) First-order reversal curve (FORC) diagrams for selected samples from the Shilou-A red clay sequence (the same samples as in Fig. 3 and 4). The FORC diagrams are scaled to their respective maximum contour density.

all consistent with enhanced pedogenesis across the MPB (Yang and Ding, 2003; Roberts, 2015; Ao et al., 2016).

Precipitation and temperature exert a primary control on pedogenic weathering (White and Blum, 1995; White et al., 1999; Wei et al., 2006; Clift et al., 2008). Increased precipitation can accelerate pedogenic weathering reactions by enhancing unsaturated soil hydrology, increasing the wetness of reactive mineral surfaces, activating stagnant porewaters that are immobile in drier soils, and decreasing soil solution concentrations and pH (White and Blum, 1995). Higher temperatures can also enhance the pedogenic weathering rate because of the thermodynamic dependence of weathering reactions (White et al., 1999). Therefore, enhanced pedogenesis across the MPB, as suggested by the Shilou Red Clay mineral magnetic record (Fig. 6a–e), is likely indicative of a climatic shift to more humid and/or warmer conditions.

A temperature increase on the CLP would be less likely and is inconsistent with observations of Antarctic glaciation and global cooling across the MPB (Zachos et al., 2001; Rommerskirchen et al., 2011; LaRiviere et al., 2012; Zhang et al., 2014). Within a context of Antarctic glaciation (Zachos et al., 2001), TEX_{86} (tetraether index of 86 carbon atoms, cf. Schouten et al. [2002]) temperature proxy data suggest that sea surface temperature (SST) in the South China Sea (Ocean Drilling Program (ODP) Site 1143) and the tropical western Pacific Ocean (ODP Site 806) decreased by ~2°C across the MPB (Zhang et al., 2014), while SST in the mid-latitude South Atlantic Ocean (ODP Site 1085) decreased by up to ~8°C (Rommerskirchen et al., 2011; Fig. 6h–j). In addition to these SST drops, decreased bottom-water temperatures have also been documented across the MPB in the Pacific and Atlantic Oceans (LaRiviere et al., 2012). Furthermore, a temperature decline is supported by increased percentages of *Pinus* and *Picea* pollen in Red Clay successions across the MPB (Ma et al., 2005). These observations indicate that the CLP was unlikely to have shifted to warmer conditions across the MPB when global climate cooled, although the possibility of regional and/or season-specific East Asian continental warming cannot be entirely excluded at present. Future independent Asian continental temperature reconstructions are crucial to test these scenarios in more detail. According to presently available evidence, we primarily relate increased pedogenesis on the CLP across the MPB to increased soil moisture availability, rather than to temperature changes.

Increased moisture availability on the CLP from the late Miocene to early Pliocene is consistent with other indications of ASM intensification. Examples include decreased eolian detrital fluxes on the CLP (Sun and An, 2002) and into the North Pacific Ocean (Rea et al., 1998), globally increased chemical weathering intensity (Filippelli, 1997), reorganization of the western Himalayan river system (Clift and Blusztajn, 2005), increased flux of clastic material to the South China Sea (Clift et al., 2014), decreased hematite/goethite ratios at ODP Site 1148 from the South China Sea (Clift, 2006), a positive shift of soil carbonate $\delta^{13}C$ from the

https://doi.org/10.1017/qua.2017.77 Published online by Cambridge University Press

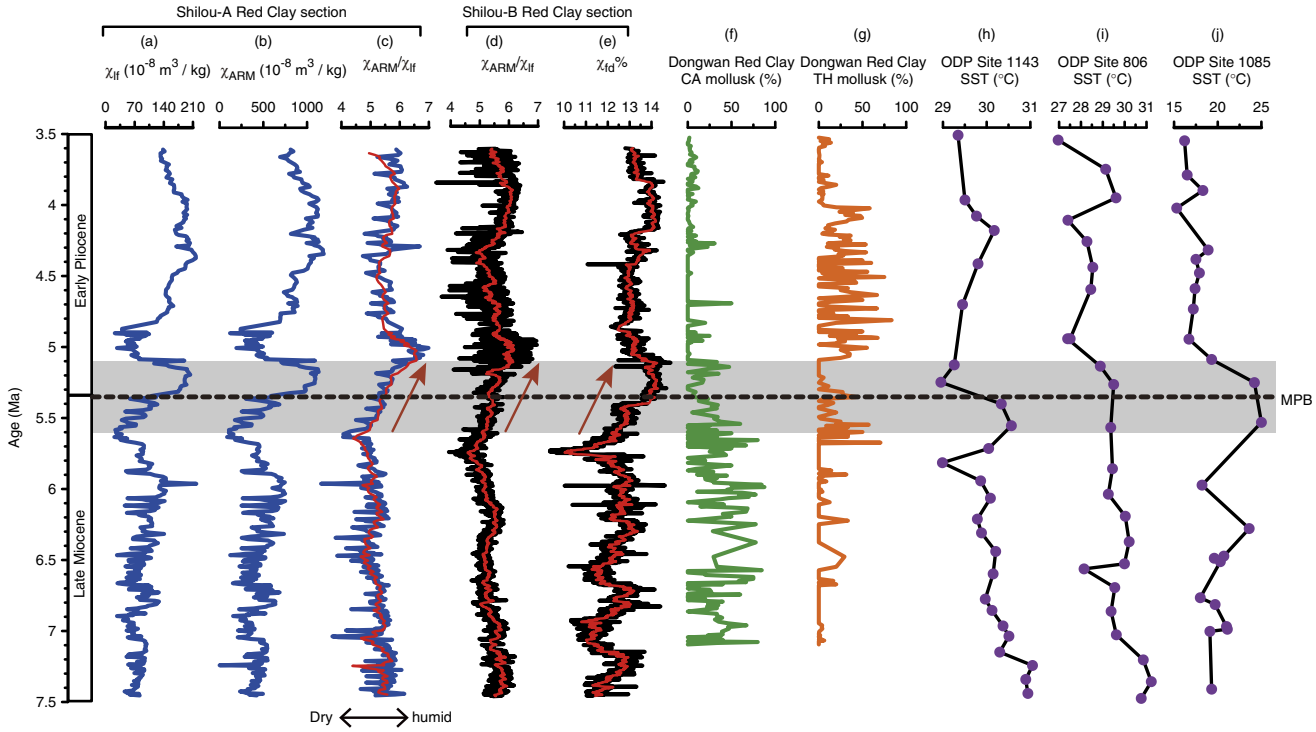

Figure 6. (color online) Changes in East Asian terrestrial climate and sea surface temperature (SST) across the Miocene-Pliocene boundary (MPB). (a–c) χ_{lf}, χ_{ARM}, and χ_{ARM}/χ_{lf} records from the Shilou-A red clay section. (d–e) χ_{ARM}/χ_{lf} and χ_{fd}% records from the Shilou-B red clay section (calculated from the raw data reported by Ao et al. (2016)). The red curves (c–e) were obtained by exponential smoothing of the raw data. (f and g) Cold-aridiphilous (CA) and thermo-humidiphilous (TH) terrestrial mollusk changes in the Dongwan red clay sequence (both from Li et al. (2008)). (h–j) TEX_{86}-based SST records from Ocean Drilling Program (ODP) sites 1143 (South China Sea), 806 (tropical western Pacific Ocean), and 1085 (mid-latitude South Atlantic Ocean; Rommerskirchen et al., 2011; Zhang et al., 2014). See text for discussion.

Siwalik Basin, and positive shifts of hydrogen (δD) and carbon ($\delta^{13}C$) isotope ratios of leaf wax C_{31} n-alkane and increased abundance of the planktonic foraminifer *Globorotalia bulloides* and the radiolarian *Actinomma* in the Arabian Sea (Quade et al., 1989; Sanyal et al., 2004; Huang et al., 2007), which are indicative of an intensified ASM. The MPB also coincides with an increase in humidity over the Mediterranean region (Eronen et al., 2009) and with increased moisture availability in tropical America, as indicated by a positive shift of black carbon $\delta^{13}C$ in the northeastern equatorial Pacific Ocean (Kim et al., 2016). The percentage of terrestrial mollusks on the CLP that prefer cold or dry environments decreases across the MPB (Fig. 6f), while the percentage of terrestrial mollusks that prefer humid or warm environments increases (Fig. 6g), which is interpreted to indicate increased ASM precipitation and/or temperature across the MPB (Li et al., 2008, 2014). Based on the aforementioned evidence, we infer that the mollusk record is more likely indicative of increased precipitation. Overall, the combined records suggest that the cooler early Pliocene had higher ASM precipitation than the warmer late Miocene (Fig. 6). This implies that increased precipitation was not always coupled with increased temperature during the late Miocene and Pliocene, in contrast to the relationship that has been inferred for the Quaternary (Lu et al., 2013; Yang et al., 2015). In addition, global cooling across the MPB may have faciliated increased moisture availability on the CLP by weakening soil water evaporation.

CONCLUSIONS

We provide a detailed new mineral magnetic record from the Shilou Red Clay sequence on the eastern CLP. The magnetic minerology of the sequence is dominated by pedogenic SP, SD, and small PSD magnetite grains. Our new mineral magnetic record suggests that both pedogenic formation of SP grains and transformation of SP grains to SD and to small PSD grains accelerated across the MPB. These are indicative of enhanced pedogenesis, which is consistent with a marked lithological color shift to redder strata across the MPB. We relate the enhanced pedogenesis to increased ASM precipitation on the CLP across the MPB. Our study suggests a notable climate shift toward more humid conditions on the CLP across the MPB, within a context of global cooling, and contributes to better understanding of late Miocene-early Pliocene Asian continental climate variability.

ACKNOWLEDGMENTS

We thank Dennis Kent for suggestions that improved the paper, Leping Yue for providing the samples used in this study, and the

https://doi.org/10.1017/qua.2017.77 Published online by Cambridge University Press

editors and anonymous reviewers for constructive comments that improved the paper. This work was supported by the National Basic Research Program of China (grant 2013CB956402), the National Natural Science Foundation of China (grants 41290253, 41420104008, 41174057, 41290250, and 41290253), the Key Research Program of Frontier Sciences, the Chinese Academy of Sciences (grants QYZDB-SSW-DQC021, QYZDY-SSW-DQC001, and ZDBS-SSW-DQC001), Australian Research Council grant DP120103952 to APR, and Australian Laureate Fellowship grant FL120100050 to EJR.

REFERENCES

An, Z.S., 2014. *Late Cenozoic Climate Change in Asia: Loess, Monsoon and Monsoon-Arid Environment Evolution*. Springer, Amsterdam.

An, Z.S., Huang, Y.S., Liu, W.G., Guo, Z.T., Clemens, S., Li, L., Prell, W, et al., 2005. Multiple expansions of C_4 plant biomass in East Asia since 7 Ma coupled with strengthened monsoon circulation. *Geology* 33, 705–708.

An, Z.S., Kukla, G.J., Porter, S.C., Xiao, J.L., 1991. Magnetic susceptibility evidence of monsoon variation on the loess plateau of central China during the last 130,000 Years. *Quaternary Research* 36, 29–36.

An, Z.S., Kutzbach, J.E., Prell, W.L., Porter, S.C., 2001. Evolution of Asian monsoons and phased uplift of the Himalaya-Tibetan plateau since Late Miocene times. *Nature* 411, 62–66.

An, Z.S., Wu, G.X., Li, J.P., Sun, Y.B., Liu, Y.M., Zhou, W.J., Cai, Y.J., et al., 2015. Global monsoon dynamics and climate change. *Annual Review of Earth and Planetary Sciences* 43, 29–77.

Anwar, T., Kravchinsky, V.A., Zhang, R., 2015. Magneto- and cyclostratigraphy in the Red Clay sequence: new age model and paleoclimatic implication for the eastern Chinese Loess Plateau. *Journal of Geophysical Research* 120, 6758–6770.

Ao, H., An, Z.S., Dekkers, M.J., Wei, Q., Pei, S.W., Zhao, H., Zhao, H.L., Xiao, G.Q., Qiang, X.K., Wu, D.C., Chang, H., 2012. High-resolution record of geomagnetic excursions in the Matuyama chron constrains the ages of the Feiliang and Lanpo Paleolithic sites in the Nihewan Basin, North China. *Geochemistry Geophysics Geosystems* 13, Q08017. http://dx.doi.org/08010.01029/02012GC004095.

Ao, H., Dekkers, M.J., Deng, C.L., Zhu, R.X., 2009. Paleoclimatic significance of the Xiantai fluvio-lacustrine sequence in the Nihewan Basin (North China), based on rock magnetic properties and clay mineralogy. *Geophysical Journal International* 177, 913–924.

Ao, H., Roberts, A.P., Dekkers, M.J., Liu, X.D., Rohling, E.J., Shi, Z.G., An, Z.S., 2016. Late Miocene-Pliocene Asian monsoon intensification linked to Antarctic ice-sheet growth. *Earth and Planetary Science Letters* 444, 75–87.

Bloemendal, J., Liu, X.M., 2005. Rock magnetism and geochemistry of two Plio-Pleistocene Chinese loess-palaeosol sequences–implications for quantitative palaeoprecipitation reconstruction. *Palaeogeography, Palaeoclimatology, Palaeoecology* 226, 149–166.

Clift, P.D., 2006. Controls on the erosion of Cenozoic Asia and the flux of clastic sediment to the ocean. *Earth and Planetary Science Letters* 241, 571–580.

Clift, P.D., Blusztajn, J., 2005. Reorganization of the western Himalayan river system after five million years ago. *Nature* 438, 1001–1003.

Clift, P.D., Hodges, K.V., Heslop, D., Hannigan, R., Van Long, H., Calves, G., 2008. Correlation of Himalayan exhumation rates and Asian monsoon intensity. *Nature Geoscience* 1, 875–880.

Clift, P.D., Wan, S.M., Blusztajn, J., 2014. Reconstructing chemical weathering, physical erosion and monsoon intensity since 25 Ma in the northern South China Sea: a review of competing proxies. *Earth-Science Reviews* 130, 86–102.

Deng, C.L., 2008. Paleomagnetic and mineral magnetic investigation of the Baicaoyuan loess-paleosol sequence of the western Chinese Loess Plateau over the last glacial-interglacial cycle and its geological implications. *Geochemistry, Geophysics, Geosystems* 9, Q04034. http:/dx.doi.org/04010.01029/02007GC001928.

Deng, C.L., Shaw, J., Liu, Q.S., Pan, Y.X., Zhu, R.X., 2006. Mineral magnetic variation of the Jingbian loess/paleosol sequence in the northern Loess Plateau of China: implications for Quaternary development of Asian aridification and cooling. *Earth and Planetary Science Letters* 241, 248–259.

Deng, C.L., Vidic, N.J., Verosub, K.L., Singer, M.J., Liu, Q.S., Shaw, J., Zhu, R.X., 2005. Mineral magnetic variation of the Jiaodao Chinese loess/paleosol sequence and its bearing on long-term climatic variability. *Journal of Geophysical Research* 110, B03103. http://dx.doi.org/03110.01029/02004JB003451.

Ding, Z.L., Xiong, S.F., Sun, J.M., Yang, S.L., Gu, Z.Y., Liu, T.S., 1999. Pedostratigraphy and paleomagnetism of a ~7.0 Ma eolian loess-red clay sequence at Lingtai, Loess Plateau, north-central China and the implications for paleomonsoon evolution. *Palaeogeography, Palaeoclimatology, Palaeoecology* 152, 49–66.

Dunlop, D.J., Özdemir, Ö., 1997. *Rock Magnetism: Fundamentals and Frontiers*. Cambridge University Press, Cambridge.

Egli, R., Chen, A.P., Winklhofer, M., Kodama, K.P., Horng, C.S., 2010. Detection of noninteracting single domain particles using first-order reversal curve diagrams. *Geochemistry Geophysics Geosystems* 11, Q01Z11. http://dx.doi.org/10.1029/2009GC002916.

Eronen, J.T., Ataabadi, M.M., Micheels, A., Karme, A., Bernor, R.L., Fortelius, M., 2009. Distribution history and climatic controls of the Late Miocene Pikermian chronofauna. *Proceedings of the National Academy of Sciences of the United States of America* 106, 11867–11871.

Evans, M.E., Heller, F., 1994. Magnetic enhancement and palaeoclimate: study of a loess/palaeosol couplet across the Loess Plateau of China. *Geophysical Journal International* 117, 257–264.

Evans, M.E., Heller, F., 2001. Magnetism of loess/palaeosol sequences: recent developments. *Earth-Science Reviews* 54, 129–144.

Evans, M.E., Heller, F., 2003. *Environmental Magnetism: Principles and Applications of Enviromagnetics*. Academic Press, New York.

Filippelli, G.M., 1997. Intensification of the Asian monsoon and a chemical weathering event in the late Miocene-early Pliocene: implications for late Neogene climate change. *Geology* 25, 27–30.

Florindo, F., Zhu, R.X., Guo, B., Yue, L.P., Pan, Y.X., Speranza, F., 1999. Magnetic proxy climate results from the Duanjiapo loess section, southernmost extremity of the Chinese loess plateau. *Journal of Geophysical Research* 104, 645–659.

Geiss, C.E., Zanner, C.W., 2006. How abundant is pedogenic magnetite? Abundance and grain size estimates for loessic soils based on rock magnetic analyses. *Journal of Geophysical Research* 111, B12S21. http://dx.doi.org/10.1029/2006JB004564.

Heller, F., Evans, M.E., 1995. Loess magnetism. *Reviews of Geophysics* 33, 211–240.

Hilgen, F.J., Lourens, L.J., van Dam, J.A., 2012. The Neogene Period. In: Gradstein, F.M., Ogg, J.G., Schmitz, M., Ogg, G. (Eds.), *The Geologic Time Scale*. Elsevier, Amsterdam, pp. 923–978.

Hu, P.X., Liu, Q.S., Torrent, J., Barrón, V., Jin, C.S., 2013. Characterizing and quantifying iron oxides in Chinese loess/paleosols: implications for pedogenesis. *Earth and Planetary Science Letters* 369, 271–283.

Huang, Y.S., Clemens, S.C., Liu, W.G., Wang, Y., Prell, W.L., 2007. Large-scale hydrological change drove the late Miocene C_4 plant expansion in the Himalayan foreland and Arabian Peninsula. *Geology* 35, 531–534.

Kim, D., Lee, Y.I., Hyeong, K., Yoo, C.M., 2016. Terrestrial biome distribution in the Late Neogene inferred from a black carbon record in the northeastern equatorial Pacific. *Scientific Reports* 6, 32847. http://dx.doi.org/32810.31038/srep32847.

Kukla, G., Heller, F., Ming, L.X., Chun, X.T., Sheng, L.T., Sheng, A.Z., 1988. Pleistocene climates in China dated by magnetic susceptibility. *Geology* 16, 811–814.

LaRiviere, J.P., Ravelo, A.C., Crimmins, A., Dekens, P.S., Ford, H.L., Lyle, M., Wara, M.W., 2012. Late Miocene decoupling of oceanic warmth and atmospheric carbon dioxide forcing. *Nature* 486, 97–100.

Li, F.J., Rousseau, D.D., Wu, N.Q., Hao, Q.Z., Pei, Y.P., 2008. Late Neogene evolution of the East Asian monsoon revealed by terrestrial mollusk record in Western Chinese Loess Plateau: from winter to summer dominated sub-regime. *Earth and Planetary Science Letters* 274, 439–447.

Li, F.J., Wu, N.Q., Rousseau, D.D., Dong, Y.J., Zhang, D., Pei, Y.P., 2014. Late Miocene-Pliocene paleoclimatic evolution documented by terrestrial mollusk populations in the western Chinese Loess Plateau. *Plos One* 9, e95754. http://dx.doi.org/10.1371/journal.pone.0095754.

Liu, Q.S., Deng, C.L., Torrent, J., Zhu, R.X., 2007. Review of recent developments in mineral magnetism of the Chinese loess. *Quaternary Science Reviews* 26, 368–385.

Liu, Q.S., Deng, C.L., Yu, Y.J., Torrent, J., Jackson, M.J., Banerjee, S.K., Zhu, R.X., 2005. Temperature dependence of magnetic susceptibility in an argon environment: implications for pedogenesis of Chinese loess/palaeosols. *Geophysical Journal International* 161, 102–112.

Liu, Q.S., Jackson, M.J., Banerjee, S.K., Maher, B.A., Deng, C.L., Pan, Y.X., Zhu, R.X., 2004. Mechanism of the magnetic susceptibility enhancements of the Chinese loess. *Journal of Geophysical Research* 109, B12107. http://dx.doi.org/12110.11029/12004JB003249.

Liu, Q.S., Jin, C.S., Hu, P.X., Jiang, Z.X., Ge, K.P., Roberts, A.P., 2015. Magnetostratigraphy of Chinese loess-paleosol sequences. *Earth-Science Reviews* 150, 139–167.

Liu, Q.S., Roberts, A.P., Larrasoaña, J.C., Banerjee, S.K., Guyodo, Y., Tauxe, L., Oldfield, F., 2012. Environmental magnetism: principles and applications. *Reviews of Geophysics* 50, RG4002. http://dx.doi.org/4010.1029/2012RG000393.

Liu, Q.S., Torrent, J., Morrás, H., Ao, H., Jiang, Z.X., Su, Y.L., 2010. Superparamagnetism of two modern soils from the northeastern Pampean region, Argentina and its paleoclimatic indications. *Geophysical Journal International* 183, 695–705.

Liu, T.S., 1985. *Loess and the Environment*. China Ocean Press, Beijing.

Liu, X.M., Rolph, T., An, Z.S., Hesse, P., 2003. Paleoclimatic significance of magnetic properties on the Red Clay underlying the loess and paleosols in China. *Palaeogeography, Palaeoclimatology, Palaeoecology* 199, 153–166.

Liu, Z.F., Liu, Q.S., Torrent, J., Barron, V., Hu, P.X., 2013. Testing the magnetic proxy χ_{FD}/HIRM for quantifying paleoprecipitation in modern soil profiles from Shaanxi Province, China. *Global and Planetary Change* 110, 368–378.

Lu, H.Y., Yi, S.W., Liu, Z.Y., Mason, J.A., Jiang, D.B., Cheng, J., Stevens, T., Xu, Z.W., Zhang, E.L., Jin, L.Y., Zhang, Z.H., Guo, Z.T., Wang, Y., Otto-Bliesner, B., 2013. Variation of East Asian monsoon precipitation during the past 21 k.y. and potential CO_2 forcing. *Geology* 41, 1023–1026.

Ma, Y.Z., Wu, F.L., Fang, X.M., Li, J.J., An, Z.S., Wang, W., 2005. Pollen record from Red Clay sequence in the central Loess Plateau between 8.10 and 2.60 Ma. *Chinese Science Bulletin* 50, 2234–2243.

Miao, Y.F., Herrmann, M., Wu, F.L., Yan, X.L., Yang, S.L., 2012. What controlled Mid-Late Miocene long-term aridification in Central Asia? Global cooling or Tibetan Plateau uplift: a review. *Earth-Science Reviews* 112, 155–172.

Muxworthy, A.R., Dunlop, D.J., 2002. First-order reversal curve (FORC) diagrams for pseudo-single-domain magnetites at high temperature. *Earth and Planetary Science Letters* 203, 369–382.

Nie, J.S., King, J., Jackson, M., Fang, X.M., Song, Y.G., 2008. AC magnetic susceptibility studies of Chinese red clay sediments between 4.8 and 4.1 Ma: paleoceanographic and paleoclimatic implications. *Journal of Geophysical Research* 113, B10106. http://dx.doi.org/10110.11029/12008JB005654.

Nie, J.S., King, J.W., Fang, X.M., 2007. Enhancement mechanisms of magnetic susceptibility in the Chinese red-clay sequence. *Geophysical Research Letters* 34, L19705. http://dx.doi.org/19710.11029/12007GL031430.

Nie, J.S., Song, Y.G., King, J.W., 2016. A review of recent advances in Red-Clay environmental magnetism and paleoclimate history on the Chinese Loess Plateau. *Frontiers in Earth Science* 4. http://dx.doi.org/10.3389/feart.2016.00027.

Nie, J.S., Song, Y.G., King, J.W., Zhang, R., Fang, X.M., 2013. Six million years of magnetic grain-size records reveal that temperature and precipitation were decoupled on the Chinese Loess Plateau during ~4.5–2.6 Ma. *Quaternary Research* 79, 465–470.

Nie, J.S., Stevens, T., Song, Y.G., King, J.W., Zhang, R., Ji, S.C., Gong, L.S., Cares, D., 2014. Pacific freshening drives Pliocene cooling and Asian monsoon intensification. *Scientific Reports* 4, 5474. http://dx.doi.org/5410.1038/Srep05474.

Qiang, X.K., Li, Z.X., Powell, C.M., Zheng, H.B., 2001. Magnetostratigraphic record of the Late Miocene onset of the East Asian monsoon, and Pliocene uplift of northern Tibet. *Earth and Planetary Science Letters* 187, 83–93.

Quade, J., Cerling, F.E., Bowman, J.R., 1989. Development of Asian monsoon revealed by marked ecological shift during the latest Miocene in northern Pakistan. *Nature* 342, 163–166.

Rea, D.K., Snoeckx, H., Joseph, L.H., 1998. Late Cenozoic eolian deposition in the North Pacific: Asian drying, Tibetan uplift, and cooling of the northern hemisphere. *Paleoceanography* 13, 215–224.

Roberts, A.P., 2015. Magnetic mineral diagenesis. *Earth-Science Reviews* 151, 1–47.

Roberts, A.P., Heslop, D., Zhao, X., Pike, C.R., 2014. Understanding fine magnetic particle systems through use of first-order reversal curve diagrams. *Reviews of Geophysics* 52, 557–602.

Roberts, A.P., Pike, C.R., Verosub, K.L., 2000. First-order reversal curve diagrams: a new tool for characterizing the magnetic properties of natural samples. *Journal of Geophysical Research* 105, 28461–28475.

https://doi.org/10.1017/qua.2017.77 Published online by Cambridge University Press

Rommerskirchen, F., Condon, T., Mollenhauer, G., Dupont, L., Schefuss, E., 2011. Miocene to Pliocene development of surface and subsurface temperatures in the Benguela Current system. *Paleoceanography* 26, PA3216. http://dx.doi.org/3210.1029/2010PA002074.

Schouten, S., Hopmans, E.C., Schefuss, E., Damste, J.S.S., 2002. Distributional variations in marine crenarchaeotal membrane lipids: a new tool for reconstructing ancient sea water temperatures? *Earth and Planetary Science Letters* 204, 265–274.

Sanyal, P., Bhattacharya, S.K., Kumar, R., Ghosh, S.K., Sangode, S.J., 2004. Mio-Pliocene monsoonal record from Himalayan foreland basin (Indian Siwalik) and its relation to vegetational change. *Palaeogeography, Palaeoclimatology, Palaeoecology* 205, 23–41.

Sun, D.H., An, Z.S., Shaw, J., Bloemendal, J., Sun, Y.B., 1998. Magnetostratigraphy and palaeoclimatic significance of late Tertiary aeolian sequences in the Chinese Loess Plateau. *Geophysical Journal International* 134, 207–212.

Sun, Y.B., An, Z.S., 2002. History and variability of Asian interior aridity recorded by eolian flux in the Chinese Loess Plateau during the past 7 Ma. *Science in China* 45, 420–429.

Verosub, K.L., Fine, P., Singer, M.J., Tenpas, J., 1993. Pedogenesis and paleoclimate: interpretation of the magnetic susceptibility record of Chinese loess-paleosol sequences. *Geology* 21, 1011–1014.

Wang, P.X., Clemens, S., Beaufort, L., Braconnot, P., Ganssen, G., Jian, Z.M., Kershaw, P., Sarnthein, M., 2005. Evolution and variability of the Asian monsoon system: state of the art and outstanding issues. *Quaternary Science Reviews* 24, 595–629.

Webster, P.J., 1994. The role of hydrological processes in ocean-atmosphere interactions. *Reviews of Geophysics* 32, 427–476.

Wei, G., Li, X.H., Liu, Y., Shao, L., Liang, X.R., 2006. Geochemical record of chemical weathering and monsoon climate change since the early Miocene in the South China Sea. *Paleoceanography* 21, PA4214. http://dx.doi.org/4210.1029/2006PA001300.

White, A.F., Blum, A.E., 1995. Effects of climate on chemical weathering in watersheds. *Geochimica et Cosmochimica Acta* 59, 1729–1747.

White, A.F., Blum, A.E., Bullen, T.D., Vivit, D.V., Schulz, M., Fitzpatrick, J., 1999. The effect of temperature on experimental and natural chemical weathering rates of granitoid rocks. *Geochimica et Cosmochimica Acta* 63, 3277–3291.

Xu, Y., Yue, L.P., Li, J.X., Sun, L., Sun, B., Zhang, J.Y., Ma, J., Wang, J.Q., 2009. An 11-Ma-old red clay sequence on the Eastern Chinese Loess Plateau. *Palaeogeography, Palaeoclimatology, Palaeoecology* 284, 383–391.

Xu, Y., Yue, L.P., Li, J.X., Sun, L., Sun, B., Zhang, J.Y., Ma, J., Wang, J.Q., 2012. Red clay deposits on the Chinese Loess Plateau during 11.0–2.6 Ma and its implications for long-term evolution of East Asian monsoon. *Environmental Earth Sciences* 66, 2021–2030.

Yang, S.L., Ding, Z.L., 2003. Color reflectance of Chinese loess and its implications for climate gradient changes during the last two glacial-interglacial cycles. *Geophysical Research Letters* 30, 2058. http://dx.doi.org/2010.1029/2003GL018346.

Yang, S.L., Ding, Z.L., Li, Y.Y., Wang, X., Jiang, W.Y., Huang, X.F., 2015. Warming-induced northwestward migration of the East Asian monsoon rain belt from the Last Glacial Maximum to the mid-Holocene. *Proceedings of the National Academy of Sciences of the United States of America* 112, 13178–13183.

Zachos, J., Pagani, M., Sloan, L., Thomas, E., Billups, K., 2001. Trends, rhythms, and aberrations in global climate 65 Ma to present. *Science* 292, 686–693.

Zhang, Y.G., Pagani, M., Liu, Z.H., 2014. A 12-million-year temperature history of the tropical Pacific Ocean. *Science* 344, 84–87.

Zhao, X., Heslop, D., Roberts, A.P., 2015. A protocol for variable-resolution first-order reversal curve measurements. *Geochemistry, Geophysics, Geosystems* 16, 1364–1377.

Zhou, L., Oldfield, F., Wintle, A.G., Robinson, S.G., Wang, J.T., 1990. Partly pedogenic origin of magnetic variations in Chinese loess. *Nature* 346, 737–739.